IIETA International Information and Engineering Technology Association
Advancing the World of Information and Engineering

International Journal of Heat and Technology
Vol. 44, No. 3, June, 2026, pp. 1004-1016
Journal homepage: http://iieta.org/journals/ijht

Thermal Performance Enhancement of Serpentine Liquid Cooling Systems for Lithium-Ion Battery Modules Using Al_2O_3 and CuO Nanofluids

Nguyen Thi Hong Ngoc[1], Nguyen Minh Chau[1*], Nguyen Trong Hieu[1], Le Van Quynh[1], Le Trach Truong[2]

[1] Faculty of Vehicle and Energy Engineering, Thai Nguyen University of Technology, Thai Nguyen 250000, Viet Nam
[2] Faculty of Mechanical Engineering, East Asia University of Technology, Bac Ninh 220000, Viet Nam

Corresponding Author Email: minhchau-ice@tnut.edu.vn

https://doi.org/10.18280/ijht.440310

Received: 20 April 2026
Revised: 7 June 2026
Accepted: 16 June 2026
Available online: 30 June 2026

Keywords:
lithium-ion battery, battery thermal management, serpentine liquid cooling, nanofluid, computational fluid dynamics

ABSTRACT

Effective thermal management is essential for maintaining the safety, durability, and performance of lithium-ion batteries (LIBs) in electric vehicles (EVs), while conventional coolants often exhibit limited heat-transfer capability. In this work, we introduce a novel numerical analysis focusing on the thermal behavior of a serpentine-channel liquid-cooled battery pack. The coolants examined include Al_2O_3/water, CuO/water, Al_2O_3/40%EG/60%Water, and CuO/40%EG/60%Water nanofluids. The simulations were carried out over a Reynolds number range of 150–750, with nanoparticle volume fractions varying from 3% to 7%. To assess cooling effectiveness, two key metrics were used: the maximum battery temperature (T_{max}) and the maximum temperature difference (ΔT_{max}). The results showed that increasing the Reynolds number and nanoparticle concentration continuously improve the thermal performance of the battery module for all investigated coolant conditions. Among the investigated cases, the 7% Al_2O_3/water nanofluid exhibited the best cooling performance, reducing T_{max} by approximately 3.02 K and ΔT_{max} by approximately 2.92 K at Re = 150 compared with pure water. Furthermore, Al_2O_3-based nanofluids consistently achieved slightly better thermal performance than CuO-based nanofluids under identical operating conditions. These findings demonstrate that employing nanofluids in serpentine cooling configurations can effectively enhance the thermal management capabilities of lithium-ion battery modules for EV applications.

1. INTRODUCTION

The inevitable trend in the transportation sector to protect the environment is the replacement of traditional vehicles powered by internal combustion engines with electric vehicles (EVs) [1]. EVs increasingly rely on lithium-ion batteries (LIBs) as their primary power source, thanks to their high energy and power densities and long operational lifespans [2]. For most LIB types, the ideal operating temperature range is 20–40 °C. Additionally, temperature differences within the battery pack should be kept at 5 °C or less [3, 4]. However, LIBs generate significant heat during operation, which can adversely affect performance, lifespan, and safety [5]. Therefore, a well-designed battery thermal management system (BTMS) is essential to preserve the optimal temperature range and reduce hazards associated with excessive heat. Recently, research and development efforts have focused on four principal BTMS categories according to the cooling medium employed: air cooling, liquid cooling, phase change material (PCM) cooling, and heat pipe cooling [6].

Air cooling systems are simple and cost-effective; however, their relatively low heat-transfer capability limits their application in high-power EV battery systems [7]. Although PCM cooling delivers efficient passive temperature control, it frequently adds extra weight and expense [8-11]. Recent studies have also explored hybrid BTMSs that combine PCM cooling with optimization techniques to improve thermal regulation and temperature uniformity. However, issues related to system complexity, increased weight, and practical implementation remain important challenges for large-scale EV applications. Heat pipe cooling is highly effective, but it remains prohibitively expensive for large-scale EV applications [12]. Liquid cooling systems, in contrast, have proven both practical and scalable, which is why they are increasingly adopted for LIB thermal control.

Immersing battery cells directly in a coolant, known as direct liquid cooling, can achieve outstanding temperature uniformity. However, risks related to coolant leakage, short circuits, and electrochemical side reactions have limited its practical application in EV systems [13]. In contrast, indirect liquid-cooling systems, such as tube-based, cold-plate, and mini- and microchannel cooling structures, offer improved safety and easier implementation. Recent studies have extensively investigated the optimization of liquid-cooled BTMSs using advanced surrogate-based and multi-objective optimization methods to improve cooling performance and battery temperature uniformity [14-17].

In addition to channel optimization, improving coolant thermal properties is another effective strategy for enhancing

BTMS performance. Due to their chemical inertness, low cost, and antifreeze properties, conventional fluids such as water and water-glycol blends are commonly used in automotive cooling systems [18]. Nevertheless, these coolants typically exhibit poor thermal conductivity, a drawback that limits the overall heat transfer capability of the BTMS [19]. Nanofluids, engineered mixtures where nanoparticles are suspended in a base liquid, have gained growing attention as a solution to this problem [20]. Thanks to their superior thermal conductivity and enhanced convective heat transfer, nanofluids have been shown in recent literature reviews to improve battery cooling markedly. Nevertheless, several significant issues persist, including nanoparticle stability, particle settling, increased pressure drop, and economic viability over extended operation periods [20]. Mondal et al. [21] reported that the use of nanofluids leads to effective improvements in heat dissipation and thermal evenness for LIBs. Sarchami et al. [22] showed that AgO nanofluids reduced the peak battery temperature and temperature difference by up to 4.83 ℃ and 1.17 ℃, respectively, during a 5C discharge process. Wiriyasart et al. [23] demonstrated that nanofluid cooling in corrugated mini-channels reduced the maximum battery temperature by up to 28.65% compared with conventional cooling systems. Other studies involving Al_2O_3 nanofluids in wavy/stair channels [24] and serpentine cooling channels [25] also demonstrated noticeable reductions in battery temperature and improved thermal uniformity. Furthermore, mono and hybrid nanofluids have shown significant enhancement in convective heat transfer and thermo-hydraulic performance for microchannel-based battery cooling systems [26].

Although previous studies have demonstrated that nanofluids can effectively reduce both the maximum battery temperature and temperature non-uniformity in lithium-ion BTMSs, several important gaps remain. Most existing studies have primarily focused on a single nanoparticle type or a single base fluid under specific cooling channel configurations, such as wavy or mini-channel structures. Consequently, direct comparisons between different nanofluids and coolant compositions under identical operating conditions remain limited.

In addition, although water-based nanofluids generally offer favorable cooling performance, practical EV cooling systems often employ ethylene glycol/water (EG/W) mixtures due to their antifreeze properties and operational reliability across varying environmental conditions. However, comprehensive comparative investigations involving both water-based and EG/W-based nanofluids for serpentine-cooled cylindrical battery modules remain scarce.

To address the research gaps identified above, this work performs a numerical analysis of the thermal response of an 80-cell cylindrical LIB pack featuring a serpentine liquid-cooling loop. The coolants considered are Al_2O_3/water, CuO/water, Al_2O_3/40%EG–60%Water, and CuO/40%EG–60%Water nanofluids. The simulations explore nanoparticle volume fractions of 3%, 5%, and 7% and Reynolds numbers of 150, 300, 450, 600, and 750. To assess cooling effectiveness, the maximum battery temperature (T_{max}) and the maximum temperature difference (ΔT_{max}) are computed using computational fluid dynamics (CFD) simulations in ANSYS Fluent. This work benchmarks the performance of different nanoparticle materials and coolant bases under consistent serpentine cooling-channel operating parameters. Moreover, a systematic analysis is conducted to examine how the Reynolds number and nanoparticle concentration affect the thermal behavior of the battery module. The results may provide useful insights into selecting suitable coolant configurations for practical EV BTMSs.

2. NUMERICAL SIMULATIONS

2.1 Thermophysical properties of nanofluids

To determine the thermophysical properties of the nanofluids, this study employed theoretical correlations widely recognized and extensively verified in prior nanofluid research [27-30]. As potential BTMS coolants, this study examined Al_2O_3 and CuO nanoparticles suspended in either pure water or EG/W blends. The present thermophysical property formulation follows the methodology previously validated in our earlier study on automotive radiator cooling using nanofluids [31].

The effective density of the nanofluid was determined as:

$$\rho_{nf} = \varphi\rho_p + (1-\varphi)\rho_{bf} \tag{1}$$

The effective heat capacity was calculated using:

$$(\rho C_p)_{nf} = \varphi(\rho C_p)_p + (1-\varphi)(\rho C_p)_{bf} \tag{2}$$

To estimate the nanofluid's thermal conductivity, the Maxwell model for spherical nanoparticles was applied:

$$k_{nf} = \frac{k_p + (\Phi-1)k_{bf} - \varphi(\Phi-1)(k_{bf}-k_p)}{k_p + (\Phi-1)k_{bf} + \varphi(k_{bf}-k_p)} k_{bf} \tag{3}$$

In this equation, the shape factor Φ was taken as 3, which corresponds to spherical particle geometry [32, 33].

The dynamic viscosity was then computed using Eq. (4):

$$\mu_{nf} = \mu_{bf}(123\varphi^2 + 7.3\varphi + 1) \tag{4}$$

In all equations above, the subscripts *nf*, *bf*, and *p* refer to the nanofluid, the base fluid, and the nanoparticles, respectively.

Table 1. Material properties of the investigated coolants and nanoparticles

Materials	K (W/m·K)	ρ (kg/m³)	C_p (kJ/kgK)	μ (kg/m·s)
Pure water	0.633	992	4174	0.00065
20%EG/80%W	0.58	1008	4020	0.0019
40%EG/60%W	0.412	1055.39	3502	0.00226
Al_2O_3	40	3960	773	-
CuO	33	6000	551	-
Aluminum	202.4	2719	871	-

Note: EG/W - ethylene glycol/water

In the present simulations, we considered the nanofluid as a homogeneous single-phase fluid. This modeling approach assumes that nanoparticles are uniformly dispersed, that agglomeration is insignificant, and that the flow remains laminar. Since the nanoparticle volume fractions examined in this work were relatively low, the influence of Brownian motion and particle sedimentation was considered negligible. These assumptions are commonly adopted in CFD-based nanofluid studies and have been shown to provide reasonable agreement with experimental observations for dilute nanofluids. The physical properties of all base fluids and nanoparticle materials examined in this study are listed in Table 1.

2.2 Geometry and mesh

Using ANSYS Workbench, a 3D representation of the lithium-ion battery pack integrated with a serpentine liquid-cooling channel was developed (see Figure 1). A total of 80 cylindrical lithium-ion cells are arranged within the module according to the battery pack layout. Detailed information about the cell characteristics is presented in Table 2. The detailed dimensions of the cooling channel are as follows: channel height 65 mm, width 3 mm, and wall thickness 0.7 mm (see Figure 1(b)).

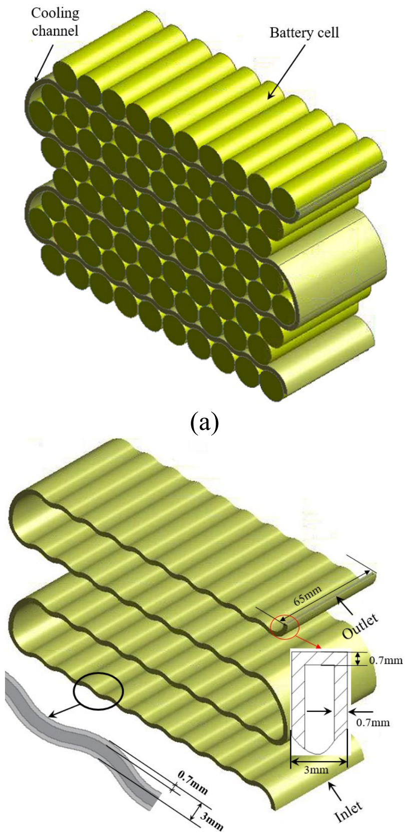

(b)

Figure 1. Computational model of the lithium-ion battery pack with an integrated serpentine liquid-cooling system: (a) overall three-dimensional layout of the battery assembly and (b) detailed dimensions of the serpentine cooling channel

Table 2. Main characteristics of the cylindrical 18650 LiFePO4 battery cell

Parameter	Description
Cell type	Cylindrical 18650
Cathode material	LiFePO4
Anode material	Graphite
Electrolyte type	Carbonate based
Rated capacity	1.35Ah
Nominal voltage	3.2 V
Cell dimensions	Diameter: 18 mm; Height: 65 mm

During cooling, the coolant enters the channel through the inlet, circulates along the serpentine flow path around the battery cells, and exits the system through the outlet. This circulation removes the heat generated during battery operation and helps maintain the module's thermal stability. To enhance heat exchange between the coolant and the cells, the simulation assumed direct thermal contact between the serpentine channel and the battery surfaces, as shown in Figure 1(b). We selected aluminum for the cooling channel due to its excellent thermal conductivity.

As part of the mesh-independence assessment, five different grid resolutions were tested, consisting of 561,543, 746,540, 967,783, 1,110,000, and 1,314,874 elements, as depicted in Figure 2(a). Figure 2(b) shows that both T_{max} and ΔT_{max} vary only slightly across the different mesh sizes. Once the element count surpasses 746,540, the deviation remains below 0.5%. To achieve an appropriate trade-off between computational cost and solution accuracy, the second mesh (746,540 elements) was chosen and employed for all subsequent simulations.

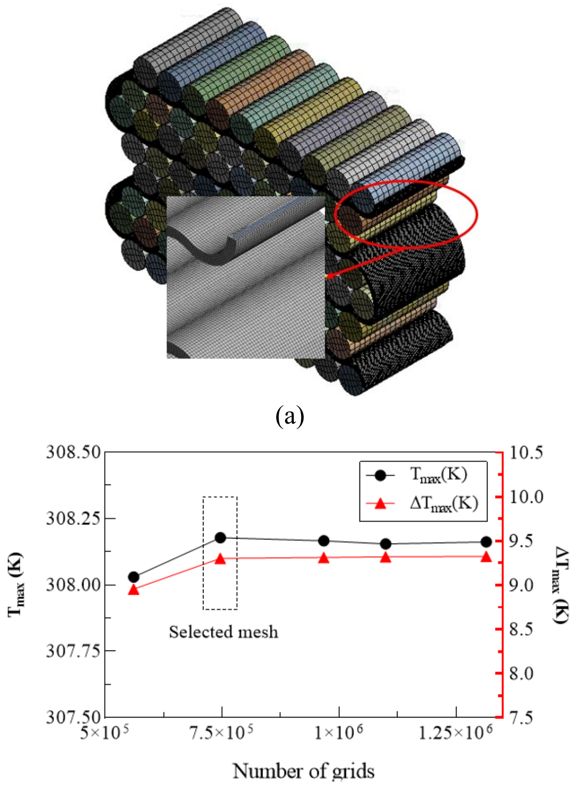

(b)

Figure 2. Mesh independence test

2.3 Governing equation

In this work, we constructed an 80-cell lithium-ion battery module and modeled the cells as uniform volumetric heat sources to reduce computational cost. The numerical model was established based on the following assumptions:

- Although heat can be transferred inside lithium-ion cells via conduction, convection, and radiation, the electrolyte is almost stationary under normal operation, with no appreciable bulk fluid movement. Hence, internal convection is negligible [15]. Additionally, within the typical operating window of −20 to 60 °C, radiative heat transfer is far less significant than conduction. As a result, the present analysis considers heat conduction as the only relevant internal heat transfer mechanism, ignoring both convection and radiation inside the cells.

- Heat transfer between adjacent cylindrical cells is assumed to be insignificant. Since neighboring cells are not in tight physical contact, the thermal contact conductance between them is very low. Previous investigations reported values on the order of 10^{-4} W/K [34], suggesting that inter-cell thermal conduction has a negligible contribution. Consequently, the generated heat is considered to be dissipated mainly through the external cooling system rather than through thermal interaction among cells.
- The material properties of the battery (such as density, heat capacity, and thermal conductivity) are assumed constant throughout the simulations. This approximation is common in battery thermal modeling, as property changes over moderate temperature ranges exert only a small effect on the overall thermal behavior.
- In addition, the present work primarily focuses on the dominant heat transfer mechanism associated with forced convection inside the liquid-cooling channel. Therefore, the aforementioned assumptions are not expected to affect the comparative optimization analysis significantly. Although slight discrepancies may occur in the prediction of absolute temperature values, the relative thermal performance trends and Pareto-optimal solutions are expected to remain reliable.

Based on the above assumptions, the governing equations describing the battery domain, the cooling channel, and the coolant flow are presented below.

The energy conservation equation of the battery can be written as:

$$\rho_b C_b \left(\frac{\partial T_b}{\partial t}\right) = \nabla(k_b \nabla T_b) + Q \quad (5)$$

Here, ρ_b, C_b, and T_b are the density, specific heat, and temperature of the lithium-ion battery, while k_b denotes its thermal conductivity. The symbol Q represents the volumetric heat generated inside the cell. During discharge, this heat production is assumed to be uniformly spread throughout the battery volume. The battery is modeled as a steady, homogeneous heat source, and the heat generation rate is obtained from the empirical relationship proposed by Bernardi et al. [35].

$$Q = \frac{I}{V_b}\left[(U_{ocv} - U) + T_b \frac{dU_{ocv}}{dT_b}\right] = \frac{1}{V_b}\left[I^2 R + I T_b \frac{dU_{ocv}}{dT_b}\right] \quad (6)$$

where, I, R, V_b charging/discharging current, internal ohmic resistance, and battery volume, respectively. The I^2R term represents irreversible Joule heating caused by the cell's internal resistance, which is taken as 0.04 Ω [36, 37]. The parameter U_{ocv} represents the open-circuit voltage of the battery.

The expression $IT_b \frac{dU_{ocv}}{dT_b}$ describes the reversible heat associated with the electrochemical reactions inside the cell, and the coefficient $IT_b \frac{dU_{ocv}}{dT_b}$ is assigned a value of 0.01116 V [36].

It should be noted that this heat-generation model does not consider additional heat sources such as side-reaction heat or polarization heat. Using Eq. (6) together with the parameters from Table 2 and literature-derived coefficients, the volumetric heat generation rates for various discharge conditions were computed and are listed in Table 3.

Table 3. Volumetric heat generation rates of the lithium-ion cell at various discharge rates

Battery Discharge Rate	Heat Generation (W/m^3)
1C	5318
2C	19452
3C	42400
4C	74163

For the serpentine cooling channel itself, the energy conservation equation takes the following form:

$$\rho_{sc} C_{sc} \left(\frac{\partial T_{sc}}{\partial t}\right) = \nabla(k_{sc} \nabla T_{sc}) \quad (7)$$

In this expression, ρ_{sc}, C_{sc}, T_{sc}, and k_{sc} correspond to the density, heat capacity, temperature, and thermal conductivity of the serpentine channel material.

The energy balance for the coolant flowing through the channel is expressed as:

$$\rho_c C_c \left(\frac{\partial T_c}{\partial t}\right) + \nabla(\rho_c C_c v T_c) = \nabla(k_c \nabla T_c) \quad (8)$$

Here, the notations ρ_c, C_c, T_c, k_c, and v stand for the coolant's density, specific heat, temperature, thermal conductivity, and velocity, in that order.

The convective heat transfer (Q_c) occurring at the solid–liquid interface between the coolant and the channel wall is determined based on Newton's cooling law: $Q_c = h_c A(T_{sc} - T_c)$, where Q_c denotes the convective heat dissipation rate, Tc represents the coolant temperature, T_{sc} is the serpentine cooling channel wall temperature; The terms h_c and A in this equation represent the convective heat transfer coefficient and the effective surface area for convective heat transfer.

To characterize the flow behavior inside the serpentine cooling channel, the Reynolds number is employed [37]:

$$R_e = \frac{\rho_c v D}{\mu} \quad (9)$$

where, ρ_c, μ, v, and D represent the coolant density, dynamic viscosity, inlet velocity, and hydraulic diameter of the channel, respectively. The thermophysical properties of the base fluids and nanoparticles employed in this study are summarized in Table 1.

The cooling system's thermal behavior was evaluated at five distinct Reynolds numbers: 150, 300, 450, 600, and 750. For each coolant, the corresponding inlet velocity was calculated using the Reynolds number formula, along with its specific thermophysical properties. As all tested Re values lie far below the typical transition threshold of 2300, the flow inside the serpentine channel was assumed to be laminar for all simulations.

Mass conservation equation is written as:

$$\nabla v = 0 \quad (10)$$

Momentum conservation equation is expressed as:

$$\rho_c \frac{dv}{dt} = -\nabla P + \mu \nabla^2 v \quad (11)$$

where, ρ_c is the coolant density, P denotes the static pressure,

μ represents the dynamic viscosity, and v is the fluid velocity vector.

2.4 Boundary conditions

To keep the computational model tractable, several assumptions together with specific boundary conditions were applied. The serpentine cooling channel was fabricated from aluminum, while pure water and nanofluids were employed as the cooling media. Every individual lithium-ion cell was treated as a uniform solid domain. Table 4 summarizes the thermophysical properties of the battery cells, aluminum, base fluids, and nanofluids.

A uniform volumetric heat generation rate of 74,163 W/m³ was applied to the battery module, corresponding to a 4C discharge rate (see Table 3). The Reynolds numbers examined in this work spanned from 150 to 750, all of which are significantly lower than the critical transition value of 2300. Consequently, laminar flow was assumed for all coolant circulation scenarios.

At the inlet, a velocity-inlet condition was specified; at the outlet, a pressure-outlet condition was used, with the gauge pressure fixed at 0 Pa. The model disregarded heat transfer from the battery module to the surrounding environment. As a result, all external boundaries of the computational domain were treated as adiabatic, i.e., no heat flux was allowed through them. The inner walls of the serpentine channel were subjected to a no-slip condition, meaning the fluid velocity at the wall was zero. The SIMPLE algorithm, which couples pressure and velocity, was employed to solve the governing equations. We considered the numerical solution converged when the normalized residuals for the continuity, momentum, and energy equations decreased below 10^{-6}.

Table 4. Material properties employed in the computational fluid dynamics (CFD) simulations

Parameter	Unit	Water	Aluminum	Battery Cell
Density, ρ	kg/m³	992	2719	2018
Specific heat, C_p	J/kg·K	4174	891	1282
Thermal conductivity, k	W/m·K	0.633	202.4	2.7
Dynamic viscosity, μ	kg/m·s	0.00065	-	-

3. RESULTS AND DISCUSSION

3.1 Simulation model validation

The numerical methodology employed here was first benchmarked against the serpentine cooling configuration documented in Xu et al. [37] before being applied to the 80-cell battery module. This validation case involved a lithium-ion battery pack featuring cylindrical 18650 LiFePO4 cells that were cooled by a serpentine channel through which water flowed.

From the reference study, we adopted the same geometry, material properties, and operational parameters: a 3C discharge rate (volumetric heat generation of 42,400 W/m³), a coolant inlet temperature of 298.15 K, and an inlet flow velocity of 0.3 m/s. Applying the identical CFD approach and boundary conditions, our simulation yielded T_{max} of 301.706 K and ΔT_{max} of 3.556 K, as shown in Figure 3.

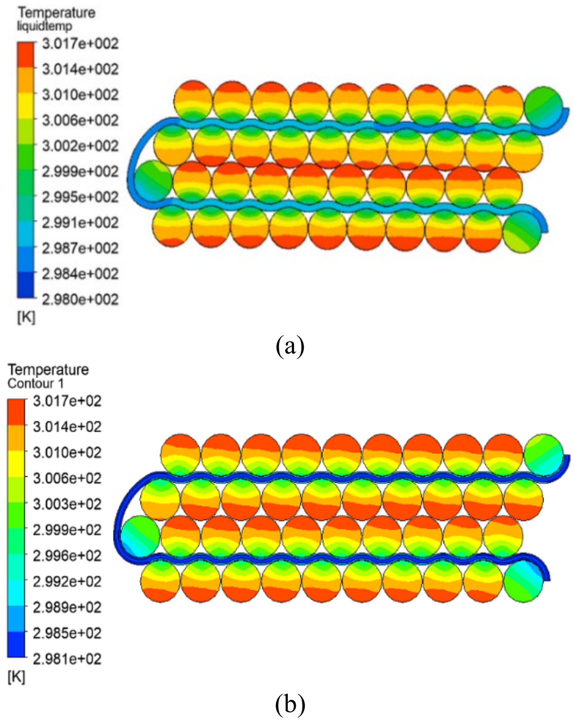

Figure 3. Validation of the present numerical model against the reference study: (a) temperature distribution predicted by Xu et al. [37] and (b) temperature distribution obtained from the current simulation

These computed values compare favorably with the numerical results of Xu et al. [37], who reported T_{max} = 301.73 K and ΔT_{max} = 3.74 K. The corresponding deviations were only 0.008% for T_{max} and 4.9% for ΔT_{max}. Therefore, the developed CFD framework was considered sufficiently accurate and reliable for subsequent simulations of the proposed 80-cell serpentine-cooled battery module.

3.2 Effect of ethylene glycol on the maximum temperature and temperature difference of cooling channel

The influence of inlet velocity and coolant type on the battery module's T_{max} and ΔT_{max} is shown in Figure 4 for three cooling fluids: pure water, 20% EG/80% water, and 40% EG/60% water. As observed, both T_{max} and ΔT_{max} increase with increasing ethylene glycol concentration at all investigated inlet velocities. Pure water outperforms the other coolants in all cases, producing the smallest temperature increase and the most even thermal distribution inside the battery module. In contrast, the 40%EG/60%Water mixture produces the highest T_{max} and ΔT_{max}, while the 20%EG/80%Water mixture exhibits intermediate behavior.

This trend is primarily associated with the thermophysical properties of the coolant mixtures. Increasing the ethylene glycol content results in higher dynamic viscosity and lower thermal conductivity, weakening the coolant's convective heat transfer and reducing the overall heat-removal performance of the serpentine cooling channel.

For all coolants tested, increasing the inlet velocity from 0.05 m/s to 0.25 m/s results in lower T_{max} and ΔT_{max} values. Higher inlet velocities enhance the convective heat transfer between the coolant and the channel wall, thereby improving heat dissipation from the battery cells and promoting a more uniform temperature distribution throughout the battery module.

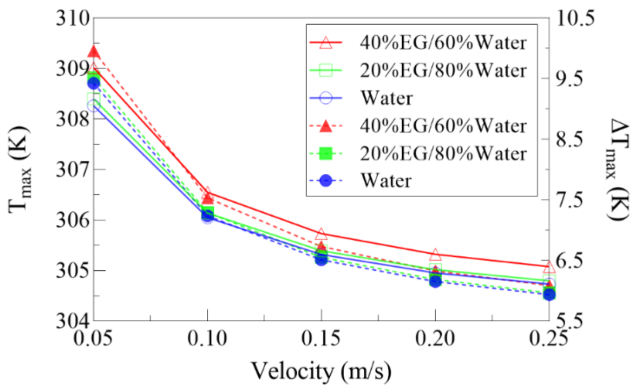

Figure 4. Effects of ethylene glycol/water (EG/W) ratio and inlet velocity on the maximum battery temperature (T_{max}) and maximum temperature difference (ΔT_{max})

3.3 Effect of nanoparticle concentration in water-based nanofluids on the thermal performance of the battery module

3.3.1 Al_2O_3/water nanofluid

The impact of both the Reynolds number and the Al_2O_3 volume fraction in water-based nanofluids on the battery's T_{max} and ΔT_{max} is presented in Figure 5. Four different coolant formulations were examined: pure water and Al_2O_3/water nanofluids at nanoparticle concentrations of 3%, 5%, and 7%.

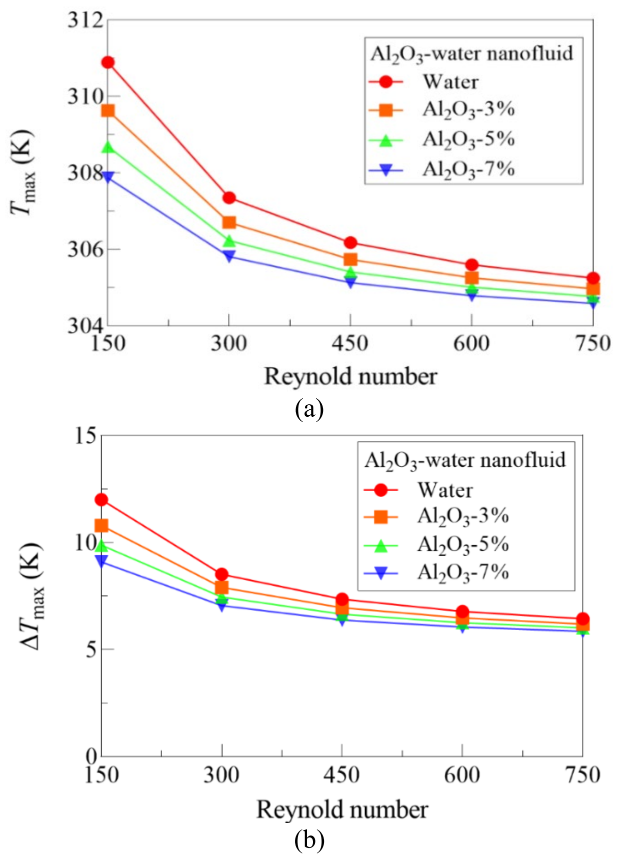

Figure 5. Effects of Reynolds number and Al_2O_3/water nanofluid concentration on the battery thermal performance: (a) maximum battery temperature (T_{max}) and (b) maximum temperature difference (ΔT_{max})

As shown in the figure, both T_{max} and ΔT_{max} decrease continuously with increasing Reynolds number for all investigated coolant conditions. A marked reduction is observed when the Reynolds number increases from 150 to 300, while the reduction rate gradually decreases at higher Reynolds numbers. This trend can be explained by improved convective heat transfer at higher flow velocities, which facilitates greater heat removal from the cells and leads to more even thermal conditions across the module.

In addition, increasing the Al_2O_3 nanoparticle concentration further enhances the cooling performance of the battery module. At a given Reynolds number, the nanofluids consistently exhibit lower T_{max} and ΔT_{max} values than pure water. Among the investigated cases, the 7% Al_2O_3/water nanofluid provides the best thermal performance over the entire Reynolds number range.

At Re = 150, the 7% Al_2O_3/water nanofluid reduces T_{max} and ΔT_{max} by approximately 3.02 K and 2.92 K (see Table 5), respectively, compared with pure water. The primary reason for these gains is the increase in thermal conductivity brought about by the Al_2O_3 nanoparticles. This enhancement enhances the coolant's convective heat transfer, thereby improving the overall performance of the serpentine cooling system.

3.3.2 CuO/water nanofluid

Figure 6 presents the effects of Reynolds number and CuO nanoparticle concentration on the thermal performance of the battery module using water-based nanofluids. Similar trends to those observed for the Al_2O_3/water nanofluid are obtained. Specifically, both T_{max} and ΔT_{max} exhibit a consistent downward trend as the Reynolds number or nanoparticle concentration increases, owing to enhanced convective heat transfer in the serpentine channel.

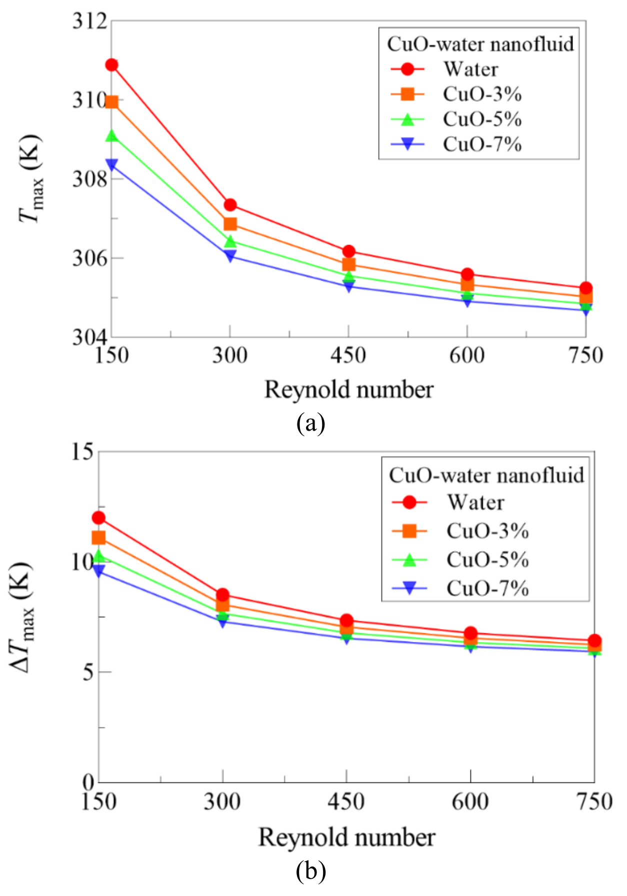

Figure 6. Effects of Reynolds number and CuO/water nanofluid concentration on the battery thermal performance: (a) maximum battery temperature (T_{max}) and (b) maximum temperature difference (ΔT_{max})

Table 5. Summary of T_{max} and ΔT_{max} values for the battery module using Al_2O_3/water nanofluids at various Reynolds numbers

Re	Water		3% Al_2O_3/water		5% Al_2O_3/water		7% Al_2O_3/water	
	T_{max} (K)	ΔT_{max} (K)	T_{max} (K)	ΔT_{max} (K)	T_{max} (K)	ΔT_{max} (K)	T_{max} (K)	ΔT_{max} (K)
150	310.89	12.01	309.63	10.79	308.69	9.89	307.87	9.09
300	307.35	8.52	306.71	7.91	306.23	7.46	305.81	7.06
450	306.18	7.36	305.74	6.95	305.41	6.65	305.13	6.39
600	305.6	6.79	305.26	6.48	305.01	6.25	304.79	6.05
750	305.25	6.44	304.97	6.2	304.77	6.01	304.59	5.85

Table 6. Summary of T_{max} and ΔT_{max} values for the battery module using CuO/water nanofluids at various Reynolds numbers

Re	Water		3% CuO/water		5% CuO/water		7% CuO/water	
	T_{max} (K)	ΔT_{max} (K)	T_{max} (K)	ΔT_{max} (K)	T_{max} (K)	ΔT_{max} (K)	T_{max} (K)	ΔT_{max} (K)
150	310.89	12.01	309.95	11.11	309.12	10.31	308.34	9.56
300	307.35	8.52	306.86	8.07	306.44	7.66	306.04	7.29
450	306.18	7.36	305.84	7.06	305.55	6.79	305.28	6.54
600	305.6	6.79	305.34	6.56	305.12	6.36	304.91	6.17
750	305.25	6.44	305.03	6.26	304.85	6.10	304.68	5.94

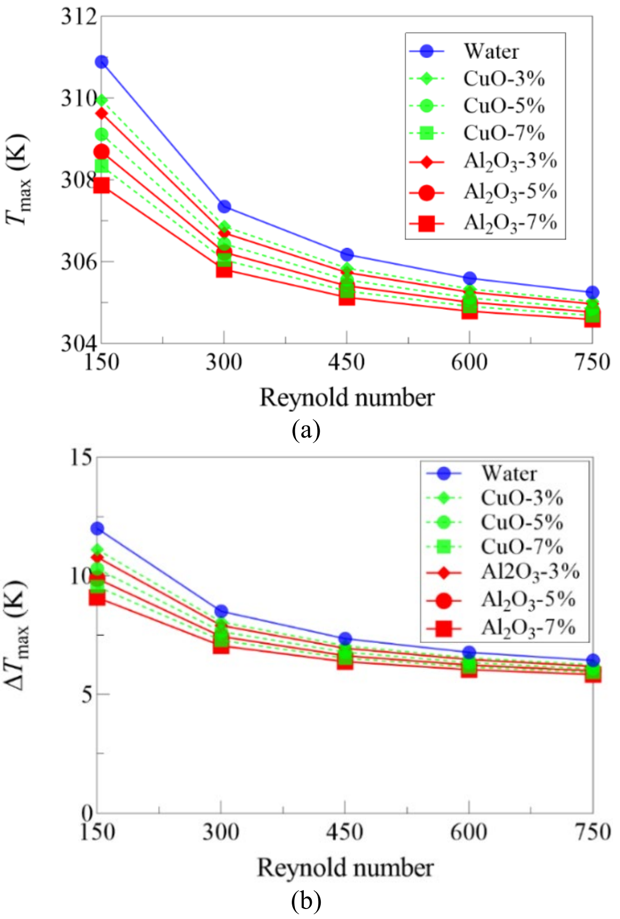

Figure 7. Comparison of thermal performance between Al_2O_3/water and CuO/water nanofluids at different Reynolds numbers: (a) maximum battery temperature (T_{max}) and (b) maximum temperature difference (ΔT_{max})

At a fixed Reynolds number, CuO/water nanofluids consistently provide lower T_{max} and ΔT_{max} values than pure water. Among the investigated cases, the 7% CuO/water nanofluid exhibits the best thermal performance. At Re = 150, T_{max} decreases from 310.89 K to 308.34 K, while ΔT_{max} decreases from 12.01 K to 9.56 K (see Table 6) compared with pure water. These correspond to reductions of approximately 2.55 K and 2.45 K, respectively, demonstrating the enhanced heat-transfer capability of the CuO/water nanofluid.

3.3.3 Comparison between Al_2O_3 and CuO nanofluids

A direct comparison between Al_2O_3/water and CuO/water nanofluids across various Reynolds numbers and nanoparticle concentrations is provided in Figure 7(a) and 7(b). Both types of nanofluids achieve lower T_{max} and ΔT_{max} than pure water.

Under identical operating conditions, the Al_2O_3/water nanofluid consistently achieves slightly better cooling performance than the CuO/water nanofluid. At the highest nanoparticle concentration of 7% and Re = 150, the Al_2O_3/water nanofluid reduces T_{max} from 308.34 K to 307.87 K and decreases ΔT_{max} from 9.56 K to 9.09 K compared with the CuO/water nanofluid. These correspond to reductions of approximately 0.47 K for both T_{max} and ΔT_{max}. Although the difference between the two nanofluids remains relatively small, the Al_2O_3/water nanofluid exhibits slightly superior thermal performance throughout the investigated range. This outcome likely stems from the collective effects of the nanofluids' thermophysical properties—such as effective thermal conductivity, viscosity, density, and convective heat transfer behavior. Furthermore, the advantage of Al_2O_3/water nanofluids is more evident at lower Reynolds numbers and higher particle concentrations, conditions where improvements in conductive heat transfer play a relatively greater role. In contrast, at higher Reynolds numbers, the thermal performance difference between the two nanofluids gradually decreased because convective heat transfer induced by coolant flow became the dominant cooling mechanism.

3.4 Effect of nanoparticle concentration in EG/water-based nanofluids on the thermal performance of the battery module

3.4.1 Al_2O_3/EG-water nanofluid

Figure 8 illustrates the effects of Reynolds number and Al_2O_3/concentration on the thermal performance of the battery module using 40%EG/60%Water-based nanofluids. The trends are qualitatively similar to those seen with water-based nanofluids: both T_{max} and ΔT_{max} fall as either the Reynolds number or the nanoparticle concentration rises. Nevertheless, the magnitude of thermal improvement is smaller, owing to the EG/water base fluid's elevated viscosity and reduced thermal conductivity.

Table 7. Summary of T_{max} and ΔT_{max} values for the battery module using Al_2O_3/40%EG-60%Water nanofluids at various Reynolds numbers

Re	40%EG/60%W		3% Al_2O_3/EG-W		5% Al_2O_3/EG-W		7% Al_2O_3/EG-W	
	T_{max}	ΔT_{max} (K)	T_{max}	ΔT_{max} (K)	T_{max}	ΔT_{max} (K)	T_{max}	ΔT_{max} (K)
150	306.48	7.47	305.99	7.03	305.65	6.72	305.34	6.44
300	305.29	6.29	305.02	6.07	304.83	5.91	304.66	5.77
450	304.89	5.90	304.69	5.75	304.55	5.64	304.43	5.54
600	304.69	5.71	304.53	5.59	304.41	5.51	304.31	5.43
750	304.57	5.59	304.43	5.49	304.33	5.43	304.25	5.36

Table 8. Summary of T_{max} and ΔT_{max} values for the battery module using CuO/40%EG-60%Water nanofluids at various Reynolds numbers

Re	40%EG/60%W		3% CuO/EG-W		5% CuO/EG-W		7% CuO/EG-W	
	T_{max}	ΔT_{max} (K)	T_{max}	ΔT_{max} (K)	T_{max}	ΔT_{max} (K)	T_{max}	ΔT_{max} (K)
150	306.48	7.47	306.09	7.13	305.78	6.85	305.49	6.59
300	305.29	6.29	305.07	6.12	304.89	5.98	304.73	5.84
450	304.89	5.90	304.72	5.78	304.59	5.68	304.48	5.59
600	304.70	5.71	304.55	5.61	304.45	5.54	304.35	5.47
750	304.58	5.59	304.45	5.51	304.36	5.45	304.28	5.39

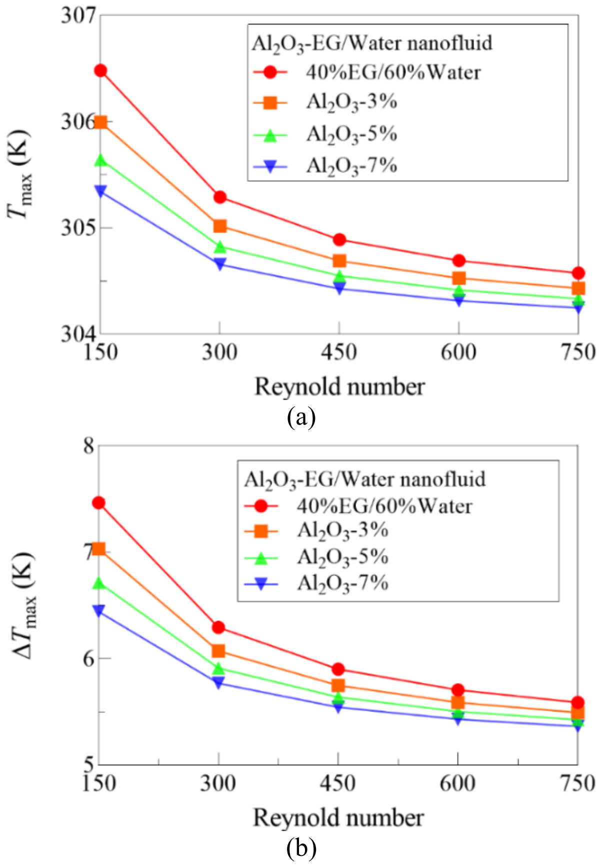

Figure 8. Effects of Reynolds number and Al_2O_3/40%EG/60%Water nanofluid concentration on the battery thermal performance: (a) maximum battery temperature (T_{max}) and (b) maximum temperature difference (ΔT_{max})

Among the investigated cases, the 7% Al_2O_3/40%EG/60%Water nanofluid provides the best thermal performance. At Re = 150, T_{max} decreases from 306.48 K to 305.34 K, while ΔT_{max} decreases from 7.47 K to 6.44 K compared with the base fluid (see Table 7). These correspond to reductions of approximately 1.14 K and 1.02 K, respectively.

3.4.2 CuO/EG-water nanofluid

Figure 9 presents the thermal performance of CuO/40%EG/60%Water nanofluids at different Reynolds numbers and nanoparticle concentrations. Similar to the Al_2O_3-based nanofluid, increasing the Reynolds number and nanoparticle concentration continuously improves the cooling performance of the battery module.

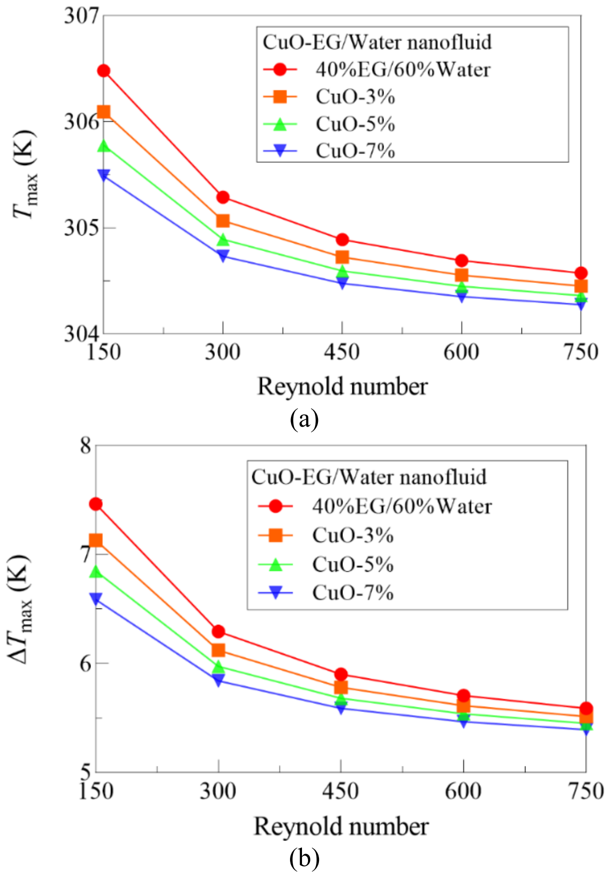

Figure 9. Effects of Reynolds number and CuO/40%EG/60%Water nanofluid concentration on the battery thermal performance: (a) maximum battery temperature (T_{max}) and (b) maximum temperature difference (ΔT_{max})

Among the investigated cases, the 7% CuO/40%EG–60%Water nanofluid achieves the lowest battery temperature and temperature difference. At Re = 150, T_{max} decreases from 306.48 K to 305.49 K, while ΔT_{max} decreases from 7.47 K to 6.59 K compared with the base fluid (see Table 8). These correspond to reductions of approximately 0.99 K and 0.88 K, respectively.

3.4.3 Comparison between Al_2O_3 and CuO nanofluids

Figure 10 shows the variations in T_{max} and ΔT_{max} of the battery module cooled by Al_2O_3/40%EG/60%Water and CuO/40%EG/60%Water nanofluids under different flow and particle concentration conditions. Both nanofluids improve the thermal management performance of the battery module compared with the EG/water base fluid, while the Al_2O_3/40%EG–60%Water consistently provides slightly lower T_{max} and ΔT_{max} values.

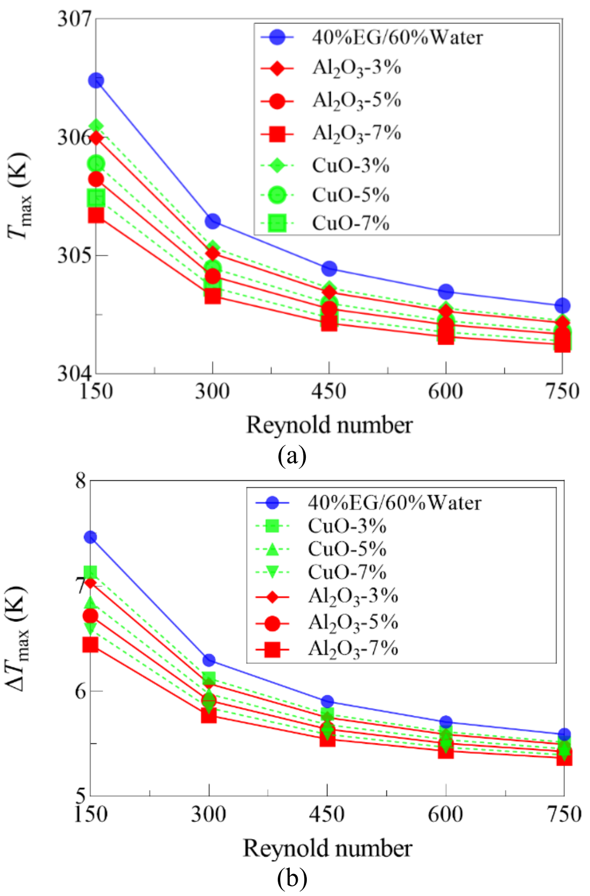

Figure 10. Comparison of thermal performance between Al_2O_3/40%EG/60%Water and CuO/40%EG/60%Water nanofluids at different Reynolds numbers: (a) maximum battery temperature (T_{max}) and (b) maximum temperature difference (ΔT_{max})

At Re = 150 and a nanoparticle concentration of 7%, the Al_2O_3/40%EG/60%Water reduces T_{max} from 305.49 K to 305.34 K and decreases ΔT_{max} from 6.59 K to 6.44 K compared with the CuO-based nanofluid. These correspond to reductions of approximately 0.15 K for both T_{max} and ΔT_{max}, indicating that the thermal performance difference between the two nanofluids remains relatively small under the investigated operating conditions.

From a practical perspective, Al_2O_3-based nanofluids may provide better long-term operational stability because alumina nanoparticles generally exhibit lower density and improved dispersion stability compared with CuO nanoparticles. Conversely, CuO-based nanofluids may offer favorable thermal conductivity enhancement but could be more susceptible to sedimentation and agglomeration during long-term operation. Therefore, the selection between Al_2O_3- and CuO-based nanofluids should consider not only cooling performance but also long-term stability and practical operating conditions in EV BTMSs.

The temperature contours inside the battery module for various coolants at Re = 150 are displayed in Figure 11. In every case examined, the battery temperature rises progressively along the coolant flow path as the fluid continuously absorbs heat as it travels through the serpentine channel. As a result, the hottest zones are found near the downstream and outlet regions, where cumulative heat uptake and diminishing temperature differences between the coolant and the battery surfaces reduce cooling effectiveness.

Compared with pure water, all nanofluid-based coolants provide lower battery temperatures and improved temperature uniformity. Among the investigated coolants, pure water exhibits the highest maximum temperature and the most pronounced thermal non-uniformity. In contrast, dispersing nanoparticles into the base fluid boosts heat removal by increasing both the thermal conductivity and the convective heat transfer capability of the coolant.

Comparing the two nanoparticle types reveals that Al_2O_3-based nanofluids have a slight edge in cooling performance under identical conditions. For instance, with water as the base fluid, T_{max} drops from about 308.34 K (CuO/water) to 307.87 K (Al_2O_3/water). Likewise, when 40%EG/60%Water is used as the base fluid, the Al_2O_3-containing nanofluid achieves the lowest T_{max} among all tested formulations, at roughly 305.34 K.

In summary, the temperature contours clearly indicate that nanofluid-based coolants, especially those containing Al_2O_3, substantially improve thermal management of the serpentine-cooled battery pack by lowering peak temperatures and enhancing thermal uniformity.

The obtained thermal trends are generally consistent with previous experimental and numerical investigations reported in the literature. In particular, [19] experimentally demonstrated that nanofluid cooling in serpentine channels enhanced heat dissipation capability and improved battery temperature uniformity compared with conventional coolants. Similar behavior was observed in the present CFD study, where increasing nanoparticle concentration and coolant flow rate continuously reduced both T_{max} and ΔT_{max}. Furthermore, the slightly superior cooling performance of Al_2O_3-based nanofluids observed in the present study is also consistent with previous investigations involving alumina nanofluids for lithium-ion battery thermal management.

The thermal performance data for all nanofluid configurations studied are compiled in Tables 5–8. Across all coolant types examined, increasing either the Reynolds number or the nanoparticle concentration consistently enhances both heat removal and temperature uniformity within the battery module. For water-based nanofluids, the Al_2O_3/water formulation generally yields marginally lower T_{max} and ΔT_{max} than its CuO/water counterpart under the same conditions. Furthermore, while nanofluids based on 40% EG/60% water do not perform as well as water-based nanofluids in absolute terms, adding nanoparticles still yields a marked improvement in cooling capacity and thermal uniformity relative to the plain EG/water-based fluid.

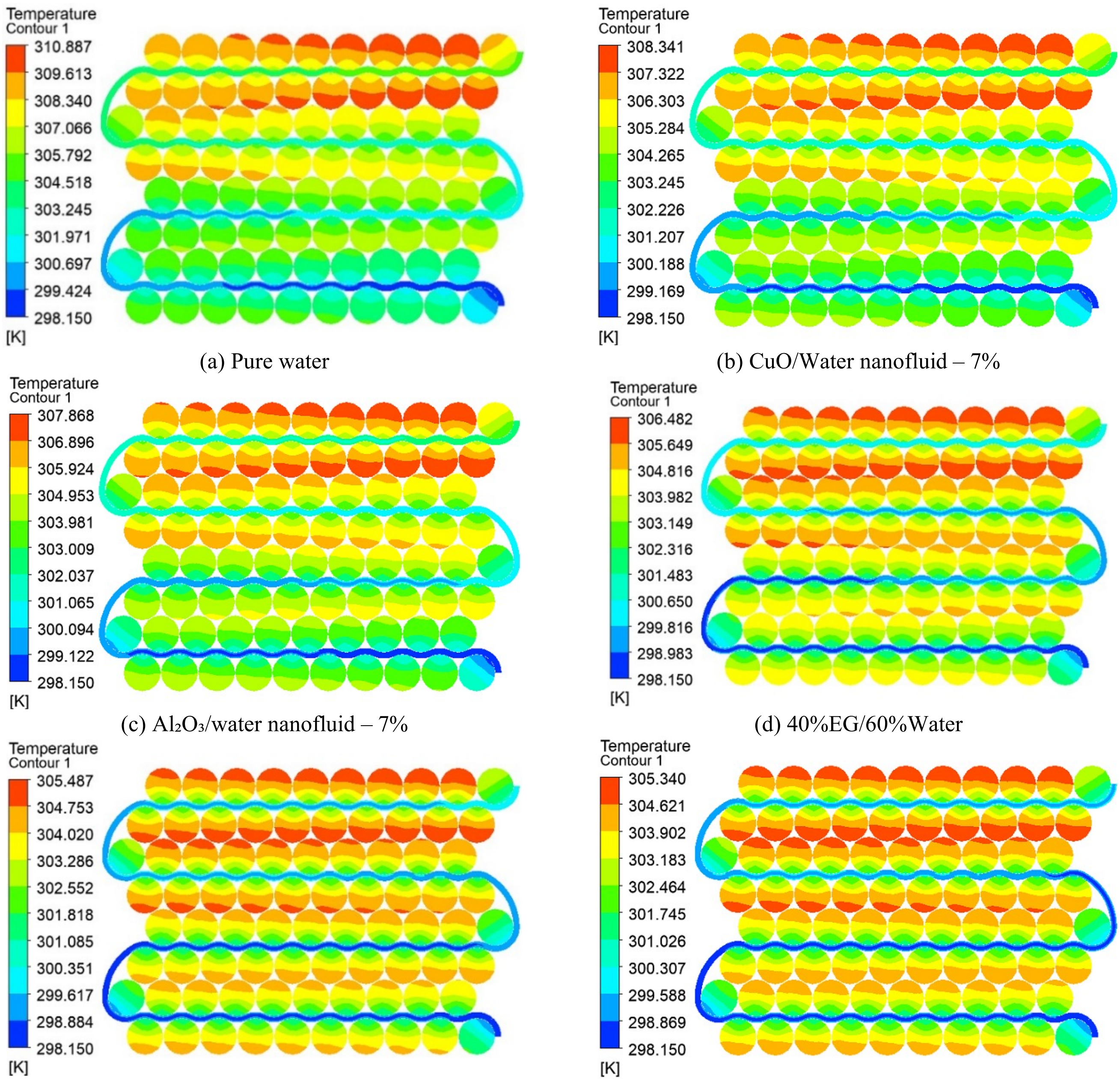

(a) Pure water (b) CuO/Water nanofluid – 7%

(c) Al_2O_3/water nanofluid – 7% (d) 40%EG/60%Water

(e) CuO-40%EG/60%Water nanofluid – 7% (f) Al_2O_3-40%EG/60%Water nanofluid – 7%

Figure 11. Temperature distributions of the battery module cooled by different base fluids and nanofluids at Re = 150
Note: As the coolant travels through the serpentine channel, it continuously extracts heat from the battery cells, resulting in a progressive increase in temperature along the flow direction. Consequently, the hottest regions are located near the downstream and outlet sections, where the accumulated thermal load and diminishing temperature difference between the fluid and cell surfaces impair heat dissipation.

4. CONCLUSIONS

This work carried out 3D numerical simulations to assess how well a serpentine liquid-cooling system performs for lithium-ion battery modules when using Al_2O_3 and CuO nanofluids dispersed in two base fluids: pure water and a 40% EG/60% water mixture. The study examined the influence of Reynolds number (150–750) and nanoparticle volume fraction (3–7%) on two key metrics: the maximum battery temperature (T_{max}) and the maximum temperature difference (ΔT_{max}). A direct comparison was made between Al_2O_3-based and CuO-based nanofluids for battery thermal management under various operating conditions.

The key findings of this study can be summarized as follows:

– For every coolant tested, raising the Reynolds number led to a marked improvement in thermal performance. Higher flow rates enhanced convective heat transfer inside the serpentine channel, resulting in continuous reductions in both T_{max} and ΔT_{max}.

– The addition of nanoparticles substantially enhanced the cooling capability of the liquid-cooling system. For both Al_2O_3/and CuO nanofluids, increasing nanoparticle concentration continuously reduced the battery temperature and improved temperature uniformity throughout the module.

– Among all investigated cases, the 7% Al_2O_3/water nanofluid exhibited the best thermal performance. At Re=150, T_{max} decreased from 310.89 K to 307.87 K, while ΔT_{max}

decreased from 12.01 K to 9.09 K compared with pure water. These correspond to reductions of approximately 3.02 K and 2.92 K, respectively.

– When 40% EG/60% water was used as the base fluid, adding nanoparticles still enhanced battery cooling. At Re = 150, the 7% Al_2O_3/40%EG–60%Water nanofluid lowered T_{max} by about 1.14 K and ΔT_{max} by about 1.02 K compared to the plain EG/water mixture.

– Under identical operating conditions, Al_2O_3-based nanofluids consistently gave marginally lower T_{max} and ΔT_{max} values than CuO-based ones. Nevertheless, the performance gap between the two remained modest across the entire range of parameters examined.

– Although pure-water-based nanofluids exhibited better absolute thermal performance than EG/water-based nanofluids, the incorporation of nanoparticles significantly improved the cooling capability of both base fluids, demonstrating the potential of nanofluid-based coolants for advanced BTMSs.

From a practical engineering perspective, the results suggest that Al_2O_3/water nanofluids operating at moderate-to-high Reynolds numbers provide the most effective cooling performance among the investigated cases for serpentine-cooled lithium-ion battery modules. In contrast, nanofluids using 40%EG/60%Water as the base fluid exhibited slightly lower thermal performance than water-based nanofluids because of the lower thermal conductivity and higher viscosity of the EG/water mixture. However, such coolant configurations may still offer practical advantages for EV applications that require antifreeze capability at low temperatures. Therefore, the selection of coolant type and operating Reynolds number should consider both thermal performance and practical operating requirements for EV BTMSs. In addition, the present CFD-based comparative framework may provide useful guidance for coolant selection and preliminary thermal design of serpentine liquid-cooling systems for EV battery applications.

The temperature distribution within the battery module became progressively more uniform along the coolant flow path, indicating effective heat removal and enhanced convective heat transfer inside the serpentine cooling channel.

While the present numerical study demonstrated noticeable improvements in battery cooling performance, several limitations remain. The simulations assumed stable and uniformly dispersed nanofluids and did not consider potential long-term effects such as nanoparticle agglomeration, sedimentation, or changes in thermophysical properties during operation. In addition, pressure drop, pumping power, and economic considerations associated with nanofluid implementation were not evaluated. Although nanofluids improved the thermal performance of the battery cooling system, increasing nanoparticle concentration may also increase coolant viscosity, pressure drop, and pumping-power requirements within the serpentine cooling channel. Furthermore, the long-term economic feasibility of implementing nanofluids, including nanoparticle preparation costs, stability maintenance, and manufacturing complexity, remains an important challenge for practical EV applications. Therefore, future studies should focus on experimental validation, thermo-hydraulic optimization, pressure-drop analysis, and long-term stability assessments to further evaluate the practical feasibility of nanofluid-based battery cooling systems for EV applications.

ACKNOWLEDGMENT

The authors wish to thank Thai Nguyen University of Technology for their valuable support throughout this study.

REFERENCES

[1] Tilly, N., Yigitcanlar, T., Degirmenci, K., Paz, A. (2024). How sustainable is electric vehicle adoption? Insights from a PRISMA review. Sustainable Cities and Society, 117: 105950. https://doi.org/10.1016/j.scs.2024.105950

[2] Ngoy, K.R., Lukong, V.T., Yoro, K.O., et al. (2025). Lithium-ion batteries and the future of sustainable energy: A comprehensive review. Renewable and Sustainable Energy Reviews, 223: 115971. https://doi.org/10.1016/j.rser.2025.115971

[3] Bao, J.T., Mao, Y., Zhang, Y.B., Xu, H., Jiang, Y.J., Yang, Y. (2024). Critical review of temperature prediction for lithium-ion batteries in electric vehicles. Batteries, 10(12): 421. https://doi.org/10.3390/batteries10120421

[4] Behi, H., Karimi, D., Behi, M., et al. (2020). Thermal management analysis using heat pipe in the high current discharging of lithium-ion battery in electric vehicles. Journal of Energy Storage, 32: 101893. https://doi.org/10.1016/j.est.2020.101893

[5] Ma, S., Jiang, M.D., Tao, P., et al. (2018). Temperature effect and thermal impact in lithium-ion batteries: A review. Progress in Natural Science: Materials International, 28(6): 653-666. https://doi.org/10.1016/j.pnsc.2018.11.002

[6] Wang, Z.C., Du, C.Q. (2021). A comprehensive review on thermal management systems for power lithium-ion batteries. Renewable and Sustainable Energy Reviews, 139: 110685. https://doi.org/10.1016/j.rser.2020.110685

[7] Hwang, F.S., Confrey, T., Reidy, C., et al. (2024). Review of battery thermal management systems in electric vehicles. Renewable and Sustainable Energy Reviews, 192: 114171. https://doi.org/10.1016/j.rser.2023.114171

[8] Fathabadi, H. (2014). High thermal performance lithium-ion battery pack including hybrid active–passive thermal management system for using in hybrid/electric vehicles. Energy, 70: 529-538. https://doi.org/10.1016/j.energy.2014.04.046

[9] Kizilel, R., Sabbah, R., Selman, J.R., Al-Hallaj, S. (2009). An alternative cooling system to enhance the safety of Li-ion battery packs. Journal of Power Sources, 194(2): 1105-1112. https://doi.org/10.1016/j.jpowsour.2009.06.074

[10] Ling, Z.Y., Wang, F.X., Fang, X.M., Gao, X.N., Zhang, Z.G. (2015). A hybrid thermal management system for lithium ion batteries combining phase change materials with forced-air cooling. Applied Energy, 148: 403-409. https://doi.org/10.1016/j.apenergy.2015.03.080

[11] Gu, X.Y., Lei, W.B., Xi, J.C., Song, M.Q. (2024). Structural optimization and battery temperature prediction of battery thermal management system based on machine learning. Case Studies in Thermal Engineering, 62: 105207. https://doi.org/10.1016/j.csite.2024.105207

[12] Yuan, X.Z., Tang, A.K., Shan, C.X., Liu, Z.Y., Li, J.M. (2020). Experimental investigation on thermal

performance of a battery liquid cooling structure coupled with heat pipe. Journal of Energy Storage, 32: 101984. https://doi.org/10.1016/j.est.2020.101984

[13] Xia, G.D., Cao, L., Bi, G.L. (2017). A review on battery thermal management in electric vehicle application. Journal of Power Sources, 367: 90-105. https://doi.org/10.1016/j.jpowsour.2017.09.046

[14] Li, W., Garg, A., Xiao, M., Gao, L. (2021). Optimization for liquid cooling cylindrical battery thermal management system based on gaussian process model. Journal of Thermal Science and Engineering Applications, 13(2): 021015. https://doi.org/10.1115/1.4047526

[15] Su, S.S., Li, W., Li, Y.S., Garg, A., Gao, L., Zhou, Q. (2021). Multi-objective design optimization of battery thermal management system for electric vehicles. Applied Thermal Engineering, 196: 117235. https://doi.org/10.1016/j.applthermaleng.2021.117235

[16] Fan, Y.W., Wang, Z.H., Fu, T. (2021). Multi-objective optimization design of lithium-ion battery liquid cooling plate with double-layered dendritic channels. Applied Thermal Engineering, 199: 117541. https://doi.org/10.1016/j.applthermaleng.2021.117541

[17] Chau, N.M., Quynh, L.V., Quang, N.M., Ngoc, N.T.H., Cong, N.T., Hieu, N.T. (2026). Toward safe and reliable batteries: Multi-objective optimization of a serpentine cooling channel for battery thermal management using GPR and NSGA-II. Batteries, 12(4): 138. https://doi.org/10.3390/batteries12040138

[18] Jha, P., Hussain, M., Khan, M.K. (2024). Numerical evaluation of nanofluid-based indirect liquid cooling of a Li-ion battery pack using equivalent circuit model under static and dynamic loading conditions. International Communications in Heat and Mass Transfer, 159: 108079. https://doi.org/10.1016/j.icheatmasstransfer.2024.108079

[19] Wankhede, S., Pingale, A., Patil, S., Shahane, K. (2025). Experimental study of a novel nanofluid cooling system based on fly ash and serpentine channels for modular lithium-ion battery thermal control. Next Energy, 9: 100396. https://doi.org/10.1016/j.nxener.2025.100396

[20] Rashid, F.L., Al-Obaidi, M.A., Al Maimuri, N.M.L., et al. (2026). Advancements in thermal management of lithium-ion batteries: The role of nanofluids and phase change materials. Environmental Technology Reviews, 15(1): 40-75. https://doi.org/10.1080/21622515.2025.2609810

[21] Mondal, B., Lopez, C.F., Mukherjee, P.P. (2017). Exploring the efficacy of nanofluids for lithium-ion battery thermal management. International Journal of Heat and Mass Transfer, 112: 779-794. https://doi.org/10.1016/j.ijheatmasstransfer.2017.04.130

[22] Sarchami, A., Kiani, M., Najafi, M., Houshfar, E. (2023). Experimental investigation of the innovated indirect-cooling system for Li-ion battery packs under fast charging and discharging. Journal of Energy Storage, 61: 106730. https://doi.org/10.1016/j.est.2023.106730

[23] Wiriyasart, S., Hommalee, C., Sirikasemsuk, S., Prurapark, R., Naphon, P. (2020). Thermal management system with nanofluids for electric vehicle battery cooling modules. Case Studies in Thermal Engineering, 18: 100583. https://doi.org/10.1016/j.csite.2020.100583

[24] Sarchami, A., Tousi, M., Kiani, M.,et al. (2022). A novel nanofluid cooling system for modular lithium-ion battery thermal management based on wavy/stair channels. International Journal of Thermal Sciences, 182: 107823. https://doi.org/10.1016/j.ijthermalsci.2022.107823

[25] Chávez, M.D., Sullayme, D.V., Vidal, Y.S., Salazar, J.V., Canazas, J., Diaz, C. (2025). Numerical study on thermal management of electric vehicle battery cooling modules using Al_2O_3 nanofluids. International Journal of Heat and Technology, 43(1): 1-10. https://doi.org/10.18280/ijht.430101

[26] Le, T.D., Lee, M.Y. (2026). Numerical investigations on heat transfer characteristics of mono and hybrid nanofluids using microchannel cooling for 21700 batteries in electric vehicles. Micromachines, 17(4): 497. https://doi.org/10.3390/mi17040497

[27] Duangthongsuk, W., Wongwises, S. (2008). Effect of thermophysical properties models on the predicting of the convective heat transfer coefficient for low concentration nanofluid. International Communications in Heat and Mass Transfer, 35(10): 1320-1326. https://doi.org/10.1016/j.icheatmasstransfer.2008.07.015

[28] Kole, M., Dey, T.K. (2010). Viscosity of alumina nanoparticles dispersed in car engine coolant. Experimental Thermal and Fluid Science, 34(6): 677-683. https://doi.org/10.1016/j.expthermflusci.2009.12.009

[29] Peyghambarzadeh, S.M., Hashemabadi, S.H., Hoseini, S.M., Jamnani, M.S. (2011). Experimental study of heat transfer enhancement using water/ethylene glycol based nanofluids as a new coolant for car radiators. International Communications in Heat and Mass Transfer, 38(9): 1283-1290. https://doi.org/10.1016/j.icheatmasstransfer.2011.07.001

[30] Devireddy, S., Mekala, C.S.R., Veeredhi, V.R. (2016). Improving the cooling performance of automobile radiator with ethylene glycol water based TiO2 nanofluids. International Communications in Heat and Mass Transfer, 78: 121-126. https://doi.org/10.1016/j.icheatmasstransfer.2016.09.002

[31] Minh, C.N. (2025). Heat transfer enhancement using Al_2O_3, CuO, and hybrid Al_2O_3–CuO nanofluids in water and ethylene glycol–water mixtures in an automotive radiator. International Journal of Heat and Technology, 43(4): 1429-1438. https://doi.org/10.18280/ijht.430420

[32] Qi, W.H., Wang, M.P., Liu, Q.H. (2005). Shape factor of nonspherical nanoparticles. Journal of Materials Science, 40: 2737-2739. https://doi.org/10.1007/s10853-005-2119-0

[33] Wang, J., Yang, X., Klemeš, J.J., Tian, K., Ma, T., Sunden, B. (2023). A review on nanofluid stability: Preparation and application. Renewable and Sustainable Energy Reviews, 188: 113854. https://doi.org/10.1016/j.rser.2023.113854

[34] Zhao, C.R., Sousa, A.C.M., Jiang, F.M. (2019). Minimization of thermal non-uniformity in lithium-ion battery pack cooled by channeled liquid flow. International Journal of Heat and Mass Transfer, 129: 660-670. https://doi.org/10.1016/j.ijheatmasstransfer.2018.10.017

[35] Bernardi, D., Pawlikowski, E., Newman, J. (1985). A general energy balance for battery systems. Journal of

The Electrochemical Society, 132(1): 5-12. https://doi.org/10.1149/1.2113792
[36] Huang, Y.Q., Lu, Y.J., Huang, R., et al. (2017). Study on the thermal interaction and heat dissipation of cylindrical Lithium-Ion Battery cells. Energy Procedia, 142: 4029-4036. https://doi.org/10.1016/j.egypro.2017.12.321
[37] Xu, H.W., Zhang, X., Xiang, G., Li, H. (2021). Optimization of liquid cooling and heat dissipation system of lithium-ion battery packs of automobile. Case Studies in Thermal Engineering, 26: 101012. https://doi.org/10.1016/j.csite.2021.101012

NOMENCLATURE

C_P	specific heat capacity, J·kg^{-1}·K^{-1}
D	hydraulic diameter, m
h	convective heat transfer coefficient, W·m^{-2}·K^{-1}
k	thermal conductivity, W·m^{-1}·K^{-1}
P	pressure, Pa
Q	heat generation rate, W/m^3
Re	Reynolds number
T	temperature, K
T_{max}	Maximum temperature, K
v	velocity, m·s^{-1}

Greek symbols

ΔT_{max}	maximum temperature difference, K
μ	dynamic viscosity kg·m^{-1}·s^{-1}
ρ	density, kg·m^{-3}
φ	nanoparticle volume concentration

Subscripts

b	battery
bf	base fluid
c	coolant
nf	nanofluid
sc	serpentine cooling channel

Abbreviations

BTMS	battery thermal management system
CFD	computational fluid dynamics
EG	ethylene glycol
EG/W	ethylene glycol/water
LIB	lithium-ion battery
SIMPLE	Semi-Implicit Method for Pressure-Linked Equations (algorithm)